Design of Optical Devices Using Frequency Domain Solvers

Ergun Simsek [#1], Qing H. Liu [*2]

[#] *Department of Electrical and Electronics Engineering, Bahcesehir University, Istanbul 34353 TURKEY*
[1] ergun.simsek@bahcesehir.edu.tr

[*] *Department of Electrical and Computer Engineering, Duke University, Durham, NC,27708-0291 USA*
[2] qhliu@ee.duke.edu

***Abstract*—This work deals with efficient frequency domain solvers specifically developed to design optical and plasmonic devices. Homogeneous and inhomogeneous objects embedded in multilayered media are analyzed using Method of Moment (MoM) and hybrid MoM-Finite Element Method (FEM), respectively. The capability of working with materials of complex permittivity makes these algorithms valid and useful for both microwave and optical regimes. Based on the good match between numerical results obtained with these algorithms and the ones found in the literature, we propose an optical antenna optimum for a semiconductor laser diode operating at a wavelength of 830 nm and an infrared sensor compatible with present silicon technology based optical devices.**

I. INTRODUCTION

Over the last two decades, there has been enormous progress in nanoscale fabrication and characterization techniques, which motivate many researchers around the globe to develop novel optical nano devices and apparatus. Plasmonic waveguides [1], [2], power dividers, ring resonators, directional couplers [3], optical antennas [4], [5] and filters [6] are some of those devices under intensive investigations. In the pre-fabrication stage, numerical solvers are quite helpful for researchers to select design parameters (such as material composition, dimensions, placement, etc.) for their specific problem of interest. For this purpose, time domain solvers are commonly used. However, it is very well known that time-domain methods might not be able to provide very accurate results for high-Q structures. One way to overcome this problem is using a frequency domain method.

Frequency domain solvers discretize the solution domain, build a matrix, and invert that matrix to obtain the solution. Smaller solution domain means smaller matrix, and smaller matrix means less memory to store and less CPU time to invert. This is why every single step decreasing the size of the solution domain may greatly reduce CPU time and memory requirements. In this direction, this work deals first with developing a surface integral equation (SIE) frequency domain solver based on Method of Moments to calculate electromagnetic (EM) scattered field from homogeneous objects embedded in a layered medium. Then, this SIE solver is adopted as a radiation boundary, where the volume enclosed by that boundary is meshed and solved with a finite element method (FEM) frequency domain solver. For the implementation of 3D radiation boundary condition, an artificial boundary, Γ, is applied to truncate the arbitrarily 3D shaped inhomogenous scatterer(s) from the layered medium. The FEM is applied in the interior region to calculate the field, while the method of moments is applied on the outer boundary, Γ, to relate the field and the induced current. Due to the form of the chosen basis functions and meshing, the fields and currents on the boundary for the FEM are obtained from the solution of the final matrix equation without using any interpolation. This algorithm stores the sparse and symmetric FEM matrix by using a row-indexed scheme to reach its the non-zero elements quickly for the sake of computational efficiency; and it solves for the coupled SIE-FEM matrix by using the biconjugate-gradient method that requires $O(KN^{4/3})$ CPU time and $O(N^{4/3})$ memory for the MoM part and $O(KN)$ CPU time and $O(N)$ memory for the FEM part, where N is the number of unknowns and K is the number of iterations. In addition, the CPU time for the evaluation of layered medium Green's functions is reduced by a simple interpolation technique. An important feature of the implementation is the use of wavelength dependent complex permittivity to describe metals [7], which is extremely crucial for the design and analyses of plasmonic structures and optical antennas.

The accuracy of the implementation is validated by several numerical examples demonstrating the optical near field enhancement and surface plasmon resonance of a single nanoparticle (with MoM) and multiple nanoparticles (with MoM-FEM) in a multilayered background. In this work, we present two interesting outcomes of this research: an optical antenna specifically designed for a semiconductor laser diode operating at

978-1-4244-5153-1/10/$26.00 ©2010 IEEE

a wavelength of 830 nm and an infrared sensor with present silicon technology based optical devices.

II. FORMULATION

In this section, we briefly describe the theory behind MoM, FEM, and hybrid MoM-FEM solver.

A. Method of Moments

Assume that there is an arbitrarily shaped homogeneous object with the surface S, electrical permittivity ϵ_s, and permeability μ_s. The object is located in a multilayered background. Layer-i is described by its own permittivity, permeability, and height (ϵ_i, μ_s, and h_i), where $i = 1, 2, \cdots, N_L$ and N_L is the number of layers. In order to calculate the scattered EM field from the object, one can solve for the electric field integral equations (EFIE) for the exterior and interior problems. The former can be written as follows

$$\begin{aligned}\mathbf{E} &= -j\omega\mu_i\langle\bar{\mathbf{K}}^J;\mathbf{J}\rangle \\ &+\tfrac{1}{j\omega\epsilon_i}\nabla\langle G_\Phi^{EJ},\nabla'\cdot\mathbf{J}\rangle + \langle\bar{\mathbf{G}}^{EM};\mathbf{M}\rangle\end{aligned} \tag{1}$$

where $\mathbf{J}$ and $\mathbf{M}$ are induced electric and magnetic currents, respectively, due to incident fields; ω is the angular frequency; $\bar{\mathbf{K}}^J$, G_Φ^{EJ}, $\bar{\mathbf{G}}^{EM}$ are different forms of dyadic layered medium Green's functions [8]. For the numerical solution, the unknown currents, $\mathbf{J}$ and $\mathbf{M}$, are expended in terms of the basis functions, $\mathbf{f}_n$ and $\mathbf{b}_n$, as

$$\begin{aligned}\mathbf{J}(\mathbf{r}) &= \textstyle\sum_{n=1}^{N_b} j_n\mathbf{f}_n(\mathbf{r}), \\ \mathbf{M}(\mathbf{r}) &= \textstyle\sum_{n=1}^{N_b} m_n\mathbf{b}_n(\mathbf{r}),\end{aligned} \tag{2}$$

where N_b is the number of interior edges on the surface of the object, j_n and m_n are the unknown coefficients for electric and magnetic current densities, respectively. When we apply the Galerkin type MoM, with the same type of functions for the testing $\mathbf{f}_m$ and $\mathbf{b}_m$, we obtain

$$S_m = \sum_{n=1}^{N_b} j_n\left[Z_{mn}^{(1)} + Z_{mn}^{(2)}\right] + \sum_{n=1}^{N_s} m_n Z_{mn}^{(3)} \tag{3}$$

where

$$S_m = \int_s \mathbf{f}_m\cdot E^{inc}ds, \tag{4}$$

$$Z_{mn}^{(1)} = jk_i\eta_i\int_s\int_{s'}\mathbf{f}_m\cdot\mathbf{K}^J\mathbf{f}_n ds'ds, \tag{5}$$

$$Z_{mn}^{(2)} = \frac{j\eta_i}{k_i}\int_s\int_{s'}\nabla\cdot\mathbf{f}_m\cdot G_\Phi^{EJ}\nabla'\cdot\mathbf{f}_n ds'ds, \tag{6}$$

$$\begin{aligned}Z_{mn}^{(3)} &= P.V.\textstyle\int_s\int_{s'}\mathbf{f}_m\cdot\nabla'\mathbf{G}^{EM}\times\mathbf{f}_n ds'ds \\ &-\tfrac{1}{2}\textstyle\int_s\mathbf{f}_m\cdot\mathbf{f}_n ds,\end{aligned} \tag{7}$$

where k_i and η_i wavenumber and intrinsic impedance of layer-i, respectively. EFIE for the interior problem is not provided for the sake of brevity.

The surface of the object is modeled using planar triangular patches and RWG (Rao, Wilton, Glisson) basis functions [9] are used to approximate the surface currents. For the numerical integration, Gaussian quadrature rules are followed and Duffy transformation is used for the self interaction terms. In order to reduce the CPU time for the evaluation of layered medium Green's functions, a simple interpolation technique is implemented.

B. Finite Element Method

Assume that a finite domain is discretized with tetrahedral elements and volume basis functions $\mathbf{\Phi}_n(\mathbf{r})$ to expand the unknown electric field along the whole volume. The numbers of inner and boundary edges are N_i and N_b, respectively, where $N = N_i + N_b$. Then, we can expand the unknown electric field and current as

$$\begin{aligned}\mathbf{E} = &\textstyle\sum_{n=1}^{N} E_n\mathbf{\Phi}_n(\mathbf{r}) \\ &= \textstyle\sum_{n=1}^{N_i} E_n^i\mathbf{\Phi}_n(\mathbf{r}) + \sum_{n=1}^{N_b} E_n^b\mathbf{\Phi}_n(\mathbf{r}),\end{aligned} \tag{8}$$

$$\hat{\mathbf{n}}\times\mathbf{H} = \sum_{n=1}^{N_b} j_n\mathbf{f}_n(\mathbf{r}) \tag{9}$$

Then, the weak form volume electric field integral equation can be written as

$$[\mathbf{A}' + \mathbf{B}']\mathbf{E} + \mathbf{G}\mathbf{J} = \mathbf{S}^\mathbf{i} \tag{10}$$

where E_n, J_n are unknown coefficients, S_i are source and $\mathbf{A}', \mathbf{B}', \mathbf{G}$ are stiffness matrices defined as,

$$\begin{aligned}S_i &= -jk_0\eta_0\int_v\mathbf{\Phi}_i(\mathbf{r})\cdot\mathbf{S}dv \\ A'_{i,n} &= \int_v(\mu_r^{-1}\nabla\times\mathbf{\Phi}_n(\mathbf{r}))\cdot(\nabla\times\mathbf{\Phi}_i(\mathbf{r}))dv \\ B'_{i,n} &= -\bar{\epsilon}_r k_0^2\int_v\mathbf{\Phi}_n(\mathbf{r})\cdot\mathbf{\Phi}_i(\mathbf{r})dv \\ G_{i,n} &= jw\mu_0\oint_s\mathbf{f}_n(\mathbf{r})\times\mathbf{\Phi}_i(\mathbf{r})ds\end{aligned} \tag{11}$$

Furthermore, the matrix form can be written as,

$$\mathbf{A}\mathbf{E}^\mathbf{i} + \mathbf{B}\mathbf{E}^\mathbf{b} = \mathbf{S}^\mathbf{i} \tag{12}$$

$$\mathbf{B}^\mathbf{T}\mathbf{E}^\mathbf{i} + \mathbf{C}\mathbf{E}^\mathbf{b} + \mathbf{G}\mathbf{J} = \mathbf{0} \tag{13}$$

where matrices $\mathbf{A}, \mathbf{B}$, and, $\mathbf{C}$ are sub-matrices of the stiffness matrix $\{\mathbf{A}' + \mathbf{B}'\}$.

C. Coupling FEM and MoM Matrices

By using $\mathbf{M}(\mathbf{r}) = -\hat{\mathbf{n}}\times\mathbf{E}|_s$, we can couple FEM and MoM equations as

$$\begin{bmatrix}\mathbf{A} & \mathbf{B} & \\ \mathbf{B}^T & \mathbf{C} & \mathbf{G} \\ & \mathbf{Z^{(3)}} & \mathbf{D}\end{bmatrix}\begin{bmatrix}\mathbf{E^i} \\ \mathbf{E^b} \\ \mathbf{J}\end{bmatrix} = \begin{bmatrix}\mathbf{S^i} \\ \mathbf{0} \\ \mathbf{S^e}\end{bmatrix}, \tag{14}$$

where $\mathbf{D} = \mathbf{Z^{(1)}} + \mathbf{Z^{(2)}}$. However, it should be noted that the above formulation is valid only if the FEM mesh matches MoM mesh on the boundary. In order to couple arbitrary meshes, some additional interpolation functions are required.

The matrix Eq. 14 is a straight-forward solution but not the most efficient way. In order to take advantage of having a sparse and symmetric FEM matrix, the matrix equations 3 and 14 are reformulated as follows

$$\mathbf{D}\ \mathbf{J} + \mathbf{F}\ \mathbf{E^b} = \mathbf{S^e}, \tag{15}$$

and

$$\begin{bmatrix} \mathbf{A} & \mathbf{B} \\ \mathbf{B}^T & \mathbf{C} \end{bmatrix} \begin{bmatrix} \mathbf{E}^i \\ \mathbf{E}^b \end{bmatrix} = \begin{bmatrix} 0 & 0 \\ 0 & \mathbf{G} \end{bmatrix} \begin{bmatrix} 0 \\ \mathbf{J} \end{bmatrix} + \begin{bmatrix} \mathbf{S}^i \\ 0 \end{bmatrix}, \tag{16}$$

respectively, where $\mathbf{F} = \mathbf{Z^{(3)}}$. In Eq. 15, we can leave the electric current alone on the left hand side and substitute it into Eq. 16

$$\begin{bmatrix} \mathbf{A} & \mathbf{B} \\ \mathbf{B}^T & \mathbf{C} - \mathbf{G}\mathbf{D^{-1}}\mathbf{F} \end{bmatrix} \begin{bmatrix} \mathbf{E}^i \\ \mathbf{E}^b \end{bmatrix} = \begin{bmatrix} \mathbf{S}^i \\ \mathbf{D^{-1}}\mathbf{S^e} \end{bmatrix}, \tag{17}$$

which is more compact than Eq. 14.

Since the FEM matrix is symmetric, the Hermitian of this matrix is simply its complex conjugate. Moreover, the FEM matrix is sparse. By using a row-indexed scheme [10], we can easily and efficiently reach the non-zero elements of the FEM matrix, which is a very important property for the solvers constructed on the biconjugate-gradient (BCG) method . As a result of these, it is more efficient to store the FEM and MoM matrices seperately as follows,

$$\left(\begin{bmatrix} \mathbf{A} & \mathbf{B} \\ \mathbf{B}^T & \mathbf{C} \end{bmatrix} + \begin{bmatrix} 0 & 0 \\ 0 & -\mathbf{G}\mathbf{D^{-1}}\mathbf{F} \end{bmatrix} \right) \times \begin{bmatrix} \mathbf{E}^i \\ \mathbf{E}^b \end{bmatrix} = \begin{bmatrix} \mathbf{S}^i \\ \mathbf{D^{-1}}\mathbf{S^e} \end{bmatrix}. \tag{18}$$

In this work, the biconjugate-gradient (BCG) method is used to solve the matrix equation which requires $O(KN^{4/3})$ CPU time and $O(N^{4/3})$ memory for the MoM part and, $O(KN)$ CPU time and $O(N)$ memory for the FEM part, where N is the number of unknowns and K is the number of iterations.

III. NUMERICAL RESULTS

For both examples, the experimental values for the optical constants of gold and silver are used [7].

A. An Optical Antenna

In [4], researchers studied optical antennas both experimentally and numerically. Similarly, in this work we try to design an antenna for the optimum field confinement and enhancement, assuming the laser in use works at a wavelength of 830 nm. Fig. 1 (a) shows the geometrical design parameters for the nanorods with rounded ends, which are half spheres with radius R. Between these half spheres, there is a cylinder with a radius of R and a height of L_c, and hence the total length of each nanorod is $L = L_c + 2R$. The distance between nanorod pairs is d. Fig. 1 (b) shows the MoM mesh used for SIE solution, where the surface is sampled with 60 points per wavelength sampling density.

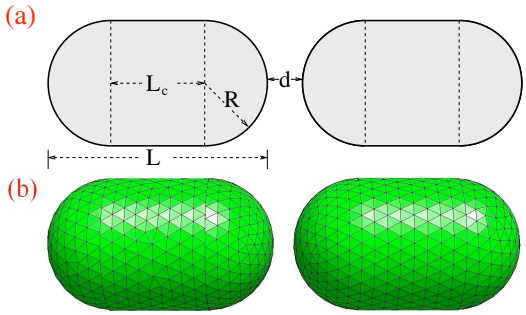

Fig. 1. Optical antenna consists of a two nanorods with rounded ends. (a) 2D view with design parameters, (b) 3D view with triangular mesh.

In order to find the optimum antenna parameters, we set R and d to a fixed value first, and then changed L_c for the range of wavelength between 600 nm and 1000 nm, and we repeat this step for several values of R and d. At the end of these simulations, we concluded that gold nanorods with $L_c = 60$ nm, $R = d = 40$ nm yields the optimum design for $\lambda = 830$ nm. Fig. 2 shows the average power recorded 300 nm above the center of the optical antenna for the range of wavelengths between 650 nm and 950 nm.

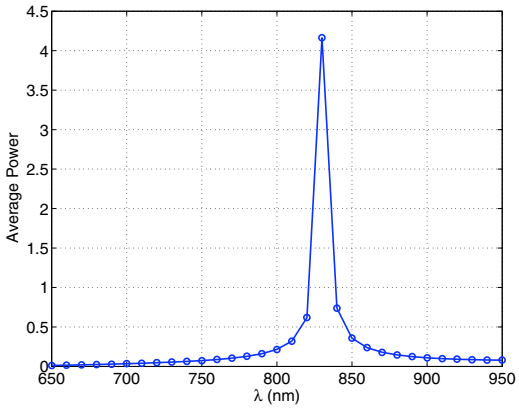

Fig. 2. Average power received 300 nm above the optical antenna for range of wavelengths between 650 nm and 950 nm for gold nanorods with $L_c = 60$ nm, $R = d = 40$ nm.

B. An Infrared Sensor

Periodically aligned metal nanoparticles are commonly used to design plasmonic sensors working in the visible light regime

[1], [2]. In this work, we investigate the possibility of such a sensor working in the infrared band. Fig. 3 shows the reflection from/transmission through a cubic silver nanoparticle array embedded on top of a silicon slide, where the dimensions of each silver cube are $1\mu m \times 1\mu m \times 0.5\mu m$, and inter-particle spacing (d, edge to edge distance) is 1μm; refractive index of the silicon is assumed to be 3.45.

In the absence of an enhanced transmission, periodic metal micro-particle array can still be used as an infrared sensor with a resonance wavelength of 2.06 μm, which can work efficiently with optically pumped semiconductor disk lasers. Another interesting result is that the reflection is less than 17% for the wavelengths shorter than $2\mu m$. Gold micro-particles provide higher transmission for the same setup and frequency range. Major outcomes of this study will be discussed in great detail at the conference.

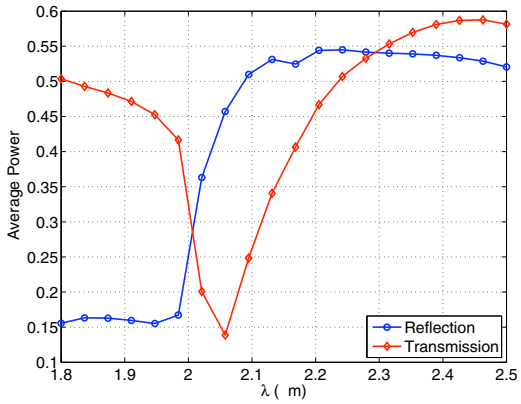

Fig. 3. Reflection from/transmission through cubic silver nanoparticle array embedded on top of a silicon slide.

IV. Conclusion

We have implemented classical frequency domain solvers and hybridized them to design optical and plasmonic devices accurately. The use of layered medium Green's functions and Lorentz-Drude model for metals enable us to work both in microwave and optical regimes. Based on the good match between numerical results obtained with these algorithms and the ones found in the literature, we propose an optical antenna optimum for a semiconductor laser diode operating at a wavelength of 830 nm and an infrared sensor compatible with present silicon technology based optical devices.

Acknowledgements

This research was supported by a Marie Curie International Reintegration Grant within the 7^{th} European Community Framework Programme. Contract No. PIRG05-GA-2009-247876.

References

[1] K. Crozier, E. Togan, E. Simsek, and T. Yang, "Experimental measurement of the dispersion relations of the surface plasmon modes of metal nanoparticle chains," *Opt. Express,* vol.15, pp. 17482–17493, 2007.

[2] E. Simsek, "Full Analytical Model for Obtaining Surface Plasmon Resonance Modes of Metal Nanoparticle Structures Embedded in Layered Media," *Opt. Express*, vol. 18, no. 2, pp: 1722–1733, Jan. 2010.

[3] D. Martin-Cano, M. Nesterov, A. Fernandez-Dominguez, F. Garcia-Vidal, L. Martin-Moreno, and E. Moreno, "Domino plasmons for subwavelength-terahertz circuitry," *Opt. Express,* vol. 18, pp. 754–764 (2010).

[4] E. Cubukcu, E.A. Kort, K.B. Crozier, and F. Capasso, "Plasmonic Laser Antenna", *Applied Physics Letters*, vol. 89 , pp. 093120, 2006.

[5] P. Bharadwaj, B. Deutsch, and L. Novotny, "Optical Antennas,"*Adv. Opt. Photon.* vol. 1, pp. 438–483, 2009.

[6] Q. Zhang, X. Huang, X. Lin, J. Tao, and X. Jin, "A subwavelength coupler-type MIM optical filter," *Opt. Express,* vol. 17, pp. 7549–7555, 2009.

[7] D. Rakic, A. B. Djurisic, J. M. Elazar and M. L. Majewski, "Optical properties of metallic films for vertical-cavity optoelectronic devices," *Appl. Opt.*, vol. 37, pp. 5271–5283, 1998.

[8] E. Simsek, Q. H. Liu, and B. Wei, "Singularity subtraction for evaluation of Green's functions for multilayer media," *IEEE Trans. Microwave Theo. and Tech.*, vol. 54, no. 1, pp. 216–225, Jan. 2006.

[9] S. Rao, D. Wilton, A. Glisson, "Electromagnetic scattering by surfaces of arbitrary shape," *IEEE Trans. Antennas Propag.,* vol. 30, no. 3, pp. 409–418, May 1982.

[10] W. H. Press, S. A. Teukolsky, W. T. Vettering, and B. P. Flannery, *Numerical Recipes in C: The Art of Scientific Computing,* 2nd edition, New York: Cambridge University Press, 1992.